Mesoscale FEM approach on cemented sands: generating and testing the digital twin

Michail Komodromos[1], *Olga* Stamati[2], and *Jürgen* Grabe[1]

[1]*Institute of Geotechnical Engineering and Construction Management, Hamburg University of Technology, Harburger Schlosssstrasse 36, 21079 Hamburg, Germany*
[2]*Univ. Grenoble Alpes, Grenoble INP, CNRS, 3SR, F-38000, Grenoble, France*
[#]*Corresponding author: michail.komodromos@tuhh.de*

ABSTRACT

The mechanics of Cemented Granular Material (CGM) have been studied by means of geotechnical experimental testing, whose output consists the basis of mathematical models which approach the material response in various loading states. The information derived from standard experimental response curves is the basis of understanding and handling the material. Still, it is intuitive to analyse the CGM down to the mesoscale and dray conclusions over the interaction of the constituent material phases. Diverging from the practice of equivalent continuum, the alternative description of a three phase composite of sand particles, cement binder and void pores has been realised in this study. In order to implement the specific morphology of this multiphase, geomaterial, X-ray Computed Tomography is used to capture the internal structure and quantify it into a three dimensional greyvalue map (or a three dimensional image). The distinction of the material phases is made possible by the application of a developed filter, which corrects the artefacts caused by beam hardening phenomena and allows for the generation of a phase segmented equivalent image. An image adapted meshing algorithm has been utilized to transform the labelled image into a tetrahedral mesh, grouped into sets that correspond to the different materials. The tetrahedral domain was assigned boundary conditions and was numerically tested under uniaxial compression using the finite element method. The kinematics of the simulation proved that the mesoscale approach, which carries internal structure information of the granular fabric and the cement paste distribution, provides a output which captures the kinematics of the granular skeleton.

Keywords: cemented sand; X-ray CT; adapted image meshing algorithm; mesoscale FEM.

1. Introduction

1.1. Macro mechanics of cemented sands

Broadly present in nature and in industrial practice, Cemented Granular Materials (CGM) have been a challening study. The addition of the supplementary phase of the binder is a factor that alters the overall mechanical response, by notably changing the stress distribution of the load sustaining stresses transmitted among the particles (Tengattini, et al. 2014), (Alavarado, Coop and Willson 2012). CGMs can be formed by various processes, according to the cementation method used, such as jet grout injection, slurry permeation to name a few. According to existing literature, the mechanical characteristics of the material are mainly dependent on the physical characteristics of the cementation degree, the relative density, the mineralogy and the geometry of the particles, but not on the production method itself (Dano, Hicher and Tailiez 2004), (Clough, Sitar and Bachus 1981) (Airey 1993). Based on this statement, a sample preparation protocol was developed, based on mixing by hand, which allows the control over the cementation degree S_{cem} and the relative density I_D. By providing the preliminary parameters of minimum and maximum void ratios (e_{min} and e_{max} respectively), an algorithm based on basic soil mechanics equations (Eqs. 1,2) computes the volume of the voids and volume of cement paste, as expressed in Eq. 3, to be mixed with the selected granular material. This procedures aids the preparation of CGM at any state of relative density and cementation.

$$e(I_D) = e_{max} - I_D \cdot (e_{max} - e_{min}) \quad (1)$$

$$V_v(e) = \frac{e \cdot V}{1 + e} \quad (2)$$

$$V_{cem} = S_{cem} \cdot V_V \quad (3)$$

The notion of the cement saturation degree of voids is used, in order to be compatible with the relative density parameter, which defines the available pore space to be filled with the cement matrix. In this work, the raw material of a model coarse sand, named Hamburger Sand (Table 1), and water diluted Portland cement, commonly known as grout milk (Rosquoët, et al. 2003), were used to produce cement sand samples in the laboratory. This samples were tested in triaxial compression under consolidated drained conditions, in order to get the principal framework of their mechanics and determine the mechanical influence of the cementation degree.

Table 1. Basic Properties of Hamburger Sand (Nagula, Grabe and Mayanja 2018).

Min Void Ratio [-]	0.526
Max Void Ratio [-]	0.813
Friction Angle [°]	32
Particle Size [mm]	1-2

The triaxial testing captures the fracturing process provoked by the presence of the binding mortar (Fig. 1), as occured in the cases of soft rocks and stifff clays. Specifically, soon after the peak stress, an evident magnitude drop occurs, leading the deviatoric stress to the residual strength which is given by the residual friction angle of the sand particles, as already affirmed in existing bibliography (Dano, Hicher and Tailiez 2004), (Clough, Sitar and Bachus 1981). Supplementary to the stress evidence, the volumetric strain response suggests that the stress drop is accompanied by a sudden and steep expansion of the sample, which is followed by constant volume response. The combination of these two simultaneous incidents rationally suggest that macro cracking emerges. This conclusion is confirmed in all cases by visual post experiment inspection, where a clear fracture band is noticed.

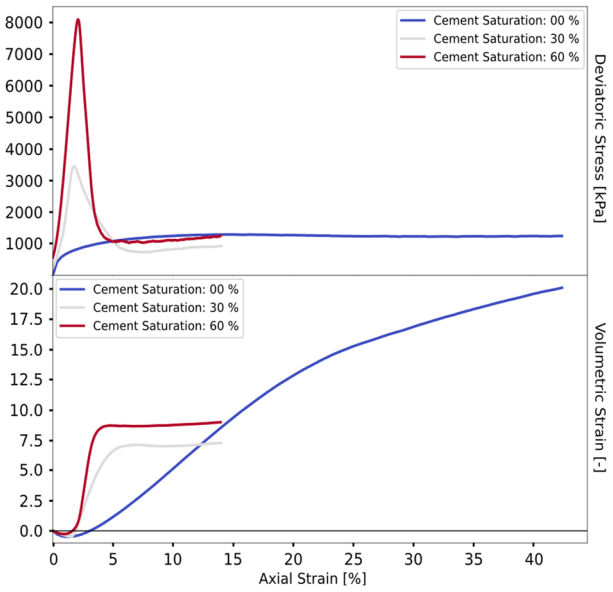

Figure 1. Influence of cementation on natural sand.

By testing the CGM under different modes of cementation, the response curves derived suggest that increased cementation shifts the material behavior to brittle. The response becomes more linear before the peak and the volumetric response is restricted, until the point of failure. The volumetric expansion associated with the emerge of macro cracks is greater in larger cementation degrees. The combination of the aforementioned facts confirms to the principle that the binder restricts granular rearrangement (macroscopically conceived as *plasticity*) and renders its deformation as a crucial parameter that defines the composite.

1.2. Micro mechanics of cemented sands

Despite the fact that triaxial compression testing provides the essential quantitative data to characterize CGMs under various cementation degrees, it is not able to capture the meso mechanical aspects of the material, which define its overall response. Although some exceptional works have been published indicating validated constitutive law formulations capable of incorporating these micro mechanical aspects as captured by full field measurements (Tengattini, et al. 2014), (Das, et al. 2014), the micro mechanics of cemented sand remain an open problem, allowing various investigation approaches, based either on continuum or discrete element method concepts (Cundall and Strack 1979). Among numerous material descriptive variables, one valuable parameter that can be incorporated and facilitate the micro mechanical display of the granular material is the morphology of the internal structure (Fig. 2). This information can be derived from three-dimensional image data, as provided by X-ray CT scanning, which is able to capture this morphology quantitatively and non-destructively (Desrues, Viggiani and Bésuelle 2010).

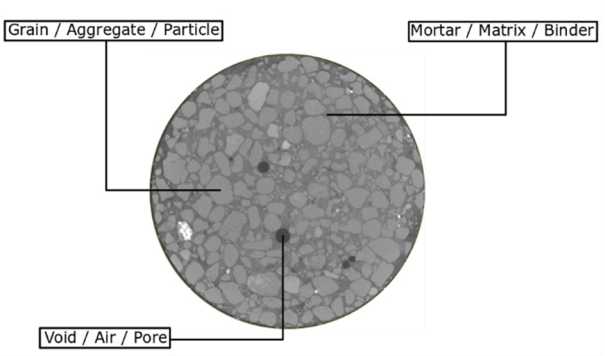

Figure 2. Mesoscale composite display.

The analysis of the aforementioned image output is an investigation chapter on its own, as the volumes that are associated with each phase are not trivially distinguished and grouped. In the case studied, the attenuation of the emitted radiation experiences artefacts. The introduced bias leads to grey values defined by the position of the voxel, apart from the material phase that it corresponds to. The segmentation cannot be realized by directly imposing threshold values. This problem was countered by developing a grey value alignment filter. It results in an enhanced image that can be labelled by imposing lower and upper thresholding values. In order to pass the information to numerical simulation, the data needs to be converted in a form which is compatible with the used numerical method.

The three-dimensional array representation of the image does not match the discretized domain (*mesh*) input required by the Finite Element Method (FEM), which is adopted in this study. In order to surpass this obstacle in the communication between images and solvers, a meshing algorithm is applied on the images, able to generate an adapted structured grid, twin to the original image. The attempt of applying the above mesoscale approach, is chosen in the current paper, by acquiring the image of a small (20 mm:10 mm)

cylindrical sample (Fig. 3). The existing elements were grouped according to the material that they correspond and assigned linear elastic properties. In addition, the interface between mortar and grains was assigned perfect fixity, assuming no detachment or slippage. By imposing the boundary conditions that correspond to the uniaxial compression test, numerical tests are carried out, providing kinematic output corresponding to the actual full field kinematic response of the material.

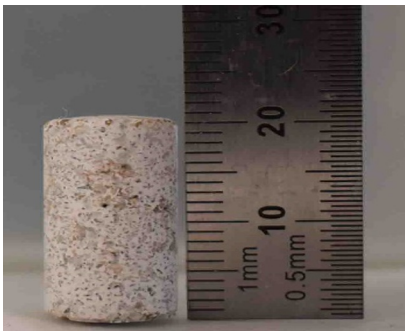

Figure 3. Mini cemented sand sample.

2. Mesoscale composite display

2.1. Interaction between material and X-rays

X-rays are a form of electromagnetic radiation which is able to pass through targeted matter. During this penetration process, the material attenuates the energy carried by the emitted beam according to its density. This crucial property is considered as the key aspect that allows the capture of a radiation attenuation map projection, displaying a view of the section of the object which is perpendicular to the direction of the emission. The aforementioned technique can be expanded to multiphase composites, whose scanning output is an image that includes regions of varying greyvalues, according to the attenuation that has taken place (Fig. 2). Due to the need of creating datasets containing three dimensional topological description of the object studied, Computed Tomography (CT) is applied. This expansion from two dimensional projections to three dimensional volumes is achieved by using algorithms based on the Radon transform (1917), which essentially enables the construction of a three-dimensional image, by composing numerous (still finite) projections, taken from consequent angular positions (Hsieh 2015). Practically, the acquisition of these projections is achieved by rotating and scanning the sample in a full circle. This paper deals with a scanning testing campaign which includes an initial capture of the internal structure of the sample. The reconstructed image output displays the trinary configuration of the composite in high resolution of 13 μm per voxel, which includes

- the phase of the grains, characterized by high attenuation values (bright on Fig. 2)
- the phase of the binding mortar, indicated by moderate attenuation values
- the phase of the voids, corresponding to low attenuation values (dark on Fig. 2)

Despite that such heterogeneities can be distinguished and comprehended by the human eye, their segmentation and grouping is not straightforward for a digital system, due to existing artefacts. Specifically, whenever X-rays penetrate a relatively dense cylindrical target, such as an mixture of Quartz sand particles and diluted cement mortar, the long path through this dense matter causes an unavoidable drop on the energy carried to photon sensor across (Fig. 4). This phenomenon introduces bias at the resulting output map, by assigning divergent values to the same phase, despite their correspondence to the same material. In addition, the presence of traces of matter of high density, such as lead or steel, results into shining artefacts which furtherly distort the image.

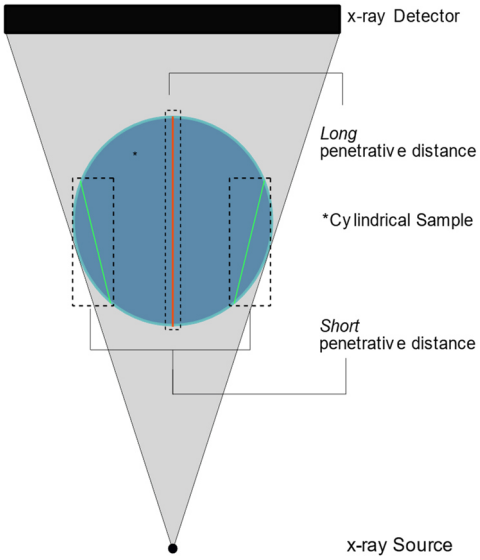

Figure 4. Scanning geometrical configuration.

A review on mesoscale studies published in literature suggests some validated segmentation solutions, which either by the physical addition of contrast enhancers (Carrara, et al. 2018), by algorithms oriented on the texture of the material via the application of the local image gradient or by applying alternative scanning modalities (neutron emission) (Stamati, et al. 2018). These techniques were applied on triphase matter that corresponded to histograms of bimodal distribution, fact indicating that labelling via direct thresholding is not possible. On the other hand, the histogram that describes the presented study remains trimodal (Fig. 5), displaying one peak for each phase, which permits an thresholding procedure (Otsu 1979).

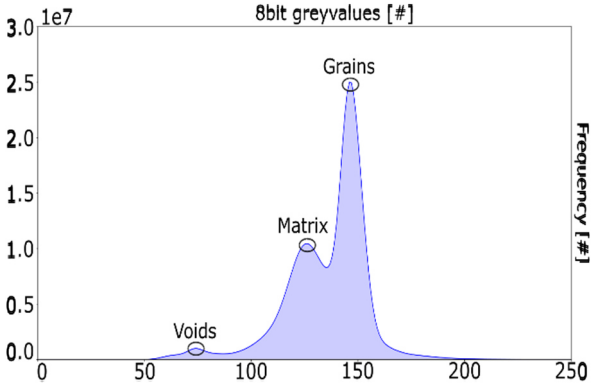

Figure 5. Trimodal histogram of CGM sample.

2.2. Against beam hardening

The inspection of the regions influenced by beam hardening suggests that the cross section is composed by a dark core, surrounded by a brighter ring. This can be better visualized in a graph, by plotting a plotline along the image. As shown in Fig. 6, these values tend to drop while moving towards the center of the image, forming a dome of darker values, making the magnitude of each voxel dependent on its the distance from the circumference. Practically, this spatial variation of the grey level leaded to the following problem; values addressed to represent aggregates placed in the center of the image turned to correspond to cement paste at the circumference. Although it may be conceived as noise, this phenomenon follows a cylindrical pattern of bias, which is the key aspect of the development by the filter presented below. The application of brute normal filtering was not considered, as it would strongly smooth the shape of the captured edges, thus deteriorate the information of the angular shape of existing heterogeneities.

In order to correct the described bias, a filter was been applied, which enlightened the dark regions, according to computed correction factors. In the first step, the image was divided into two subdomains; the bright circumferential ring and the dark core. Local grey value histogram functions were computed for each subdomain and the grey values that corresponds to the peak of the grains (Fig. 7). The difference between the grey values on each histogram determined the value that needed to be added to the voxels of the dark subdomain, in order to elevate them to the same level as these of the bright circumference.

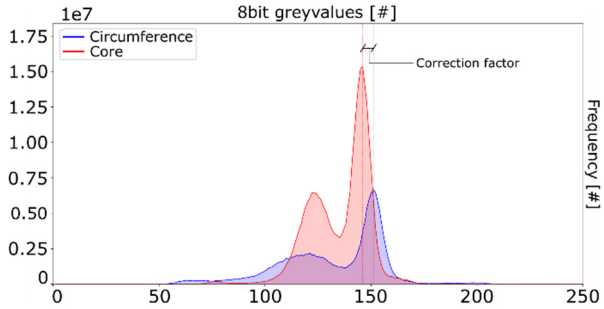

Figure 7. Local histogram comparison.

Indeed, by adding the value on the dark voxels of the core and applying a very light median filtering, the grey values corresponding to the grains were placed on the same level, along the total area of the cross section (Fig. 8).

The same alignment process was carried out on the axial direction, by decomposing the three-dimensional image into the individual vertical slices, calculating and applying the correction factors via histogram comparisons. The shining artefacts due to traces of metals or other matter of high density were wiped out, by

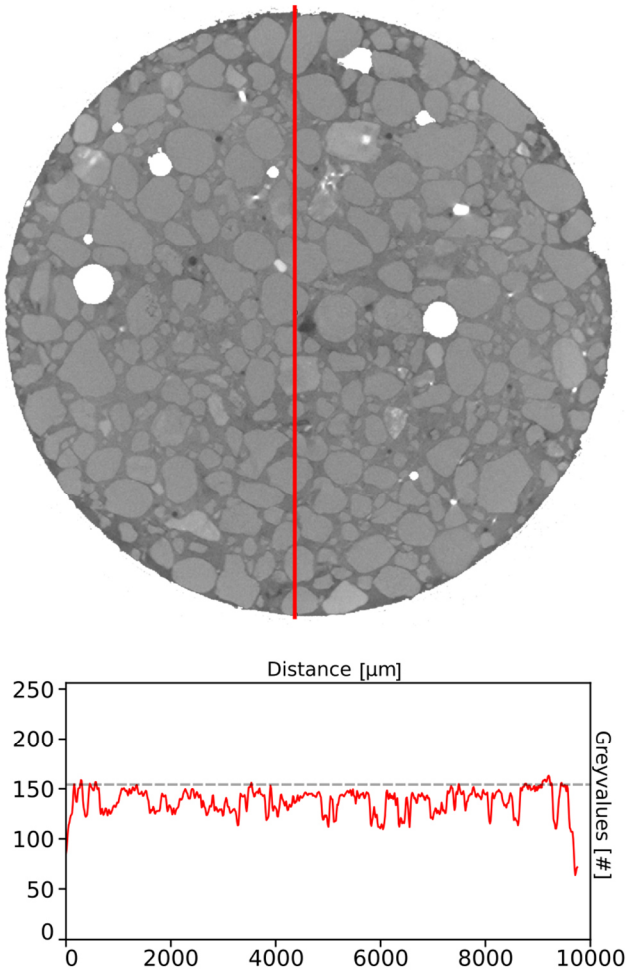

Figure 6. Image with beam hardening artefacts.

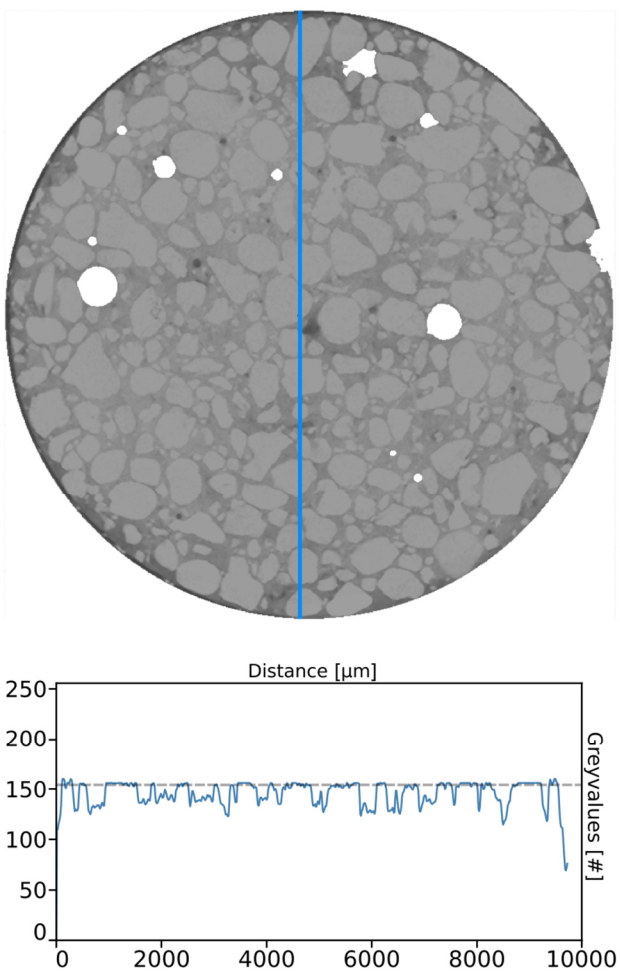

Figure 8. Image free of beam hardening artefacts.

applying a high frequency cut off filter on the values beyond the maximum peak of the histogram. The above procedure allowed the distinction between the particles and the bounding mortar, by imposing a single threshold value. Another threshold value was placed to distinguish the voids and the mortar. The selection of that value could vary in a vast range without severe consequence on the quality of the segmentation, as indicated on Fig. 5 by the wide 'valley' separating the void phase and the solid phases.

3. Image based mesh generation

3.1. Motivation and discretization concepts

The motivation behind the aforementioned image segmentation is the extraction of the geometrical information describing its substance. Despite the fact that it has ultimately been extracted, up to this point, data is still expressed in the form a three-dimensional matrix or a tagged image file format (TIFF). Such data architecture is not suited to be used as an input to a simulation. The majority of grid based numerical methods are originally formulated and developed to operate on data points (nodes), which are embedded in a mesh. This discretized approach of the continuum operates quite efficiently in small to moderate strain problems, thanks to the entity of the elements, which provides a convenient mean to apply calculus operators, such as the gradient which is essential for the solving scheme. Since the experimental evidence suggested that the mechanical response of the composite relies mainly on the deformation of the cement matrix, the Finite Element Method (FEM) has been chosen, due to its capacity of accurately capturing material deformation on small strains.

The communication between labelled images and FE solvers has been an active field of research on mesoscale approaches. Notably, in the field of geomaterials, two techniques have been addressed; the non-adapted meshing technique (from now on referred as NAMT) and the adapted meshing technique (from now on referred as AMT). The NAMT, as applied in heterogeneous quasi brittle materials (Moës, et al. 2003) and implemented in the open source code SPAM (Stamati, et al. 2020), follows the concept of casting the captured heterogeneities on an unstructured mesh. An unstructured FE mesh is created, without being adapted to the morphology that defines the scanned internal structure, but being adjusted to the overall size dimension of the domain. The computation of the distance fields of each phase included in the image provides the datasets that contain all the necessary information on the existing interfaces, which shape the heterogeneities. The distance fields are projected on the unstructured mesh, defining single and bi material elements. This concept allows single elements to define two materials, by having an embedded interface. This bi material property renders the NAMT an efficient grid generation tool and makes use of FE enrichment concepts, to deal with the interface jumps (Roubin, et al. 2014). Among others, this approach has the advantage of not requiring Delaunay refinement processes to ensure the good shape of the tetrahedra.

3.2. Adapted image meshing technique

On the other hand, the AMT produces the equivalent mesh in a slightly different way, consisting of single-phase elements adapted to the imaged morphology. The following concept has been used in this study, calling tools implemented in the highly efficient open source geometric library CGAL (Alliez P. 2022). As it has already been stated, the essential topological description of the inclusions is allocated at their edges. Considering segmented images are just discrete maps, the aforementioned description can be derived by the application of Euclidean norm of the gradient operator (Fig. 9). The result is a clear definition of the phase boundaries, which can be distinguished according to the phases that they separate (grains and mortar, mortar and air, grain and air) and consists the basis for placing the potential interface nodes (Boissonnat J.D. 2005). Afterwards, the generation of the connectivity matrix is conducted by applying the Delaunay-based triangulation algorithms to the cloud of the distributed points, producing the bulk tetrahedral elements. An additional option is the application of the same algorithm on the interface points, producing interfacial triangular elements. In order to ensure the non-distorted shape of the elements, the generated points are regulated according to a mesh optimization algorithm (Pons J.P. 2007). The above procedure provides the following feature; the exclusion of a specific phase can be explicitly commanded, by restraining the point generation function from placing nodes inside the bulk characterized by a specific label. Such attribute is quite beneficial in cases of porous materials, because it is able to naturally skipping pore voids. Instead, gaps are created in the mesh, whose interface with solids is a stress-free surface.

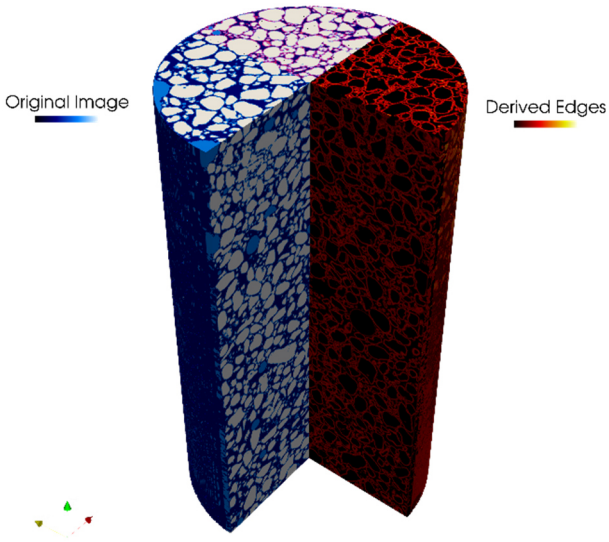

Figure 9. Match between reference and edges.

Despite the fact that the image-based grid is formed, it remains vacant in the sense that the elements are not grouped to the corresponding phase. Such sorting requires another communication process between the reference image and the mesh. Specifically, the center of gravity of every tetrahedron is considered as its reference point calculated. This coordinate is then correlated to the

equivalent voxel on the reference image, which derives the information about the corresponding phase and sends it back to the meshing algorithm, which stores the elements in groups. As the figure comparison suggests, the morphological correspondence between the two objects is satisfactory (Fig. 10). In order to quantify their divergence, the volumetric error for each phase is computed. By performing a parametric study on the error corresponding to different mesh fineness, it is evident that the choice of a decent maximum triangulation distance reduces the volumetric error down to the magnitude of 2 %.

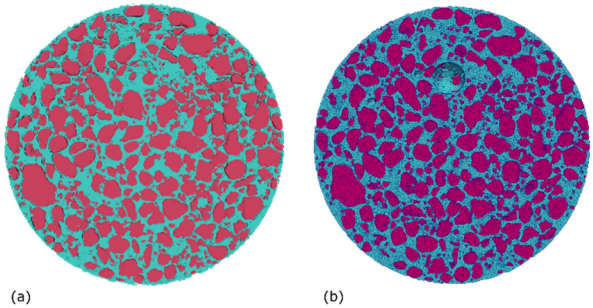

Figure 10. (a) reference image, (b) equivalent tetrahedral mesh.

4. Image based FEA

4.1. Overall FEA framework

The result of the previous preparatory work is adjusted to be imported in FE, which in the studied case is the implicit finite element code Abaqus Standard, developed and distributed by Dassault Systèmes. The reproduction of the physical uniaxial compression test requires the assignment of the physical properties that identify the constituent materials (grains and matrix) and the imposition of the equivalent boundary conditions. In contrast with physical testing, which provides axial displacement and force, under the assumption that the whole sample is described solely by one tensor, mesoscale FE provides way richer data on the *full field* response of the composite. Specifically, the current simulation provides 22.2 million tensors, with one to one correspondence to each element.

This study focuses on the linear elastic regime of the cemented sand material. While such concept does not apply efficienlty on dry or unsaturated granular materials, whose response is highly non linear from the very early strain magnitudes, highly cement saturated cemented sand presents an evidently ‘linearized’ response. This statement is confirmed by experimental data (Fig. 1) and it can be claimed that the addition of matrix suppresses plasticity, therefore pre-peak non linearities. Based on this fact, linear elasticity, along with fully coupled interfaces can be valid and is currently applied. Such decision was made in sake of simplicity, without excluding the capacity of implementing non linear constitutive laws, which can potential capture the failure modes of the constituent phases.

On the mechanical characterization of the granular phase, true uncertainty exists due to the presence of different material particles in the system. Technically, every particle is characterized by different material properties, associated with its solid substance. Nevertheless, this particle assembly is configured to be a set of Quartz sand, which has been mechanically tested and addressed to have an overall stiffness lying in the order of some GPa (Wichtmann and Triantafyllidis 2014). Therefore, a set of common elastic properties has been assigned to the granular phase (Table 2), which is the practice in the vast majority of granular based simulations. As far as the diluted mortar is concerned, its phase has been assigned a set of elastic parameters that fits the experimental output, also by making the assumption of homogeneity in the cement paste.

Table 2. Material linear elastic properties

	Particles	**Matrix**	**Voids**
Elastic Modulus [MPa]	4000	30	-
Poisson’s Ratio	0.01	0.2	-

The loading condition of the uniaxial compression test is achieved by restraining normal displacement on the bottom face and prescribing compressive displacement on the top one of the cylindrical sample (Fig. 11). Although friction phenomena at these surfaces are evident in laboratory testing, the simulation of material and plates interaction would significantly increase the computational cost and exceeds the scope of this article. In order to avoid singularities caused by rigid body motion, tangential lateral displacement restrictions is applied (Fig. 11). As already stated and also confirmed by the results, this action suppresses singularities without causing any parasitic stresses.

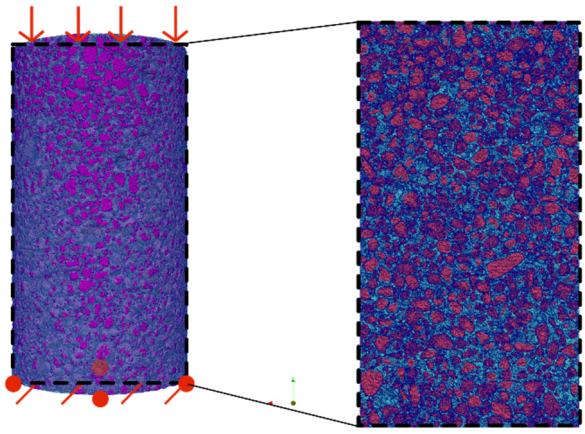

Figure 11. Prescribed boundary conditions.

4.2. Computational validation and kinematic field

On the computational aspect of the problem, the reliability of the simulation remains questionable. Mesh dependency pathogenesis is an issue concerning all FE concepts, especially the cases of highly irregular geometries and extended constituent material interaction. This emerges from the fact that the mesh fineness alters the deformation mode of the simulated system, thus the result output.

The consequence of domains lacking accuracy is excessive stiffness and inability of displaying accurately the underlying physics. The evidence required to ensure the mesh independency of the simulation is similar results after a certain point of discretization. For the sake of economy, the scalar equivalent of volumetric deformation is chosen as a representative magnitude of the response of the domain, derived for different mesh fineness applied and plotted over the existing number of nodes and elements. Evidently, the variation of the volumetric deformation with the accuracy results into reduced values, which ultimately reaches a plateau (Fig. 12). This relieving evidence suggests mesh independency of the simulation and in parallel highlights the following crucial aspect. In spite of the morphological validation, objectivity requires control and inspection over accuracy.

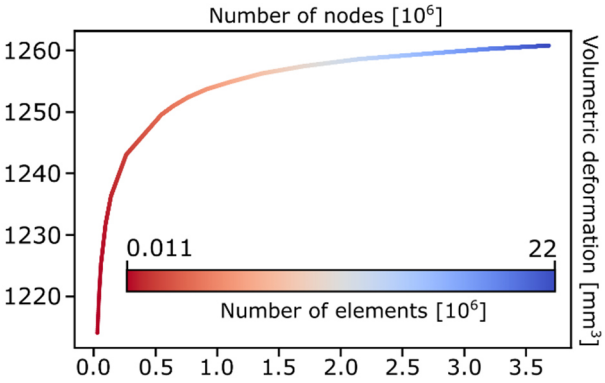

Figure 12. Mesh dependency study.

A glimpse over the full field output of axial displacement suggests that mesoscale approach is indeed a very powerful tool. Despite using purely continuum concepts, this method is able to capture granular medium concepts (Fig. 13). The patches on the overall axial displacement field are a typical characteristic of the grains, which correspond to quasi rigid bodies. In addition, the existence of voids, displayed as white dots on the contour display, defines domains attracting diverging displacements, furtherly influencing the kinematics. A visual inspection shows that generic homogeneous linear elastic domains are not able to display heterogeneity caused phenomena.

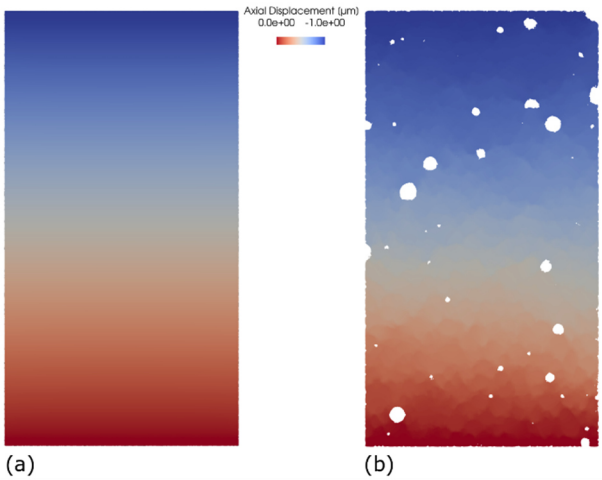

Figure 13. (a) Generic linear elasticity, (b) Mesoscale enriched linear elasticity.

The matter of accuracy in capturing granular mechanics is also displayed by a cutline plot at the center of the domain of axial displacement results. As previously mentioned, the exclusion of the pores and their replacement with stress free surfaces leads to 'gaps' in the simulation output, which fit exactly the air phase, not statically contributing to the system. Moreover, the quasi rigid body motion characterizing the grains is translated as constant displacement at the volumes where these domains are placed. The axial distribution plot over a straight cutline through the results confirm that both are evident (Fig. 14), by the time sufficient accuracy is applied. Finally, the displacement values seem to converge to a common value after evident increase in the number of DOFs.

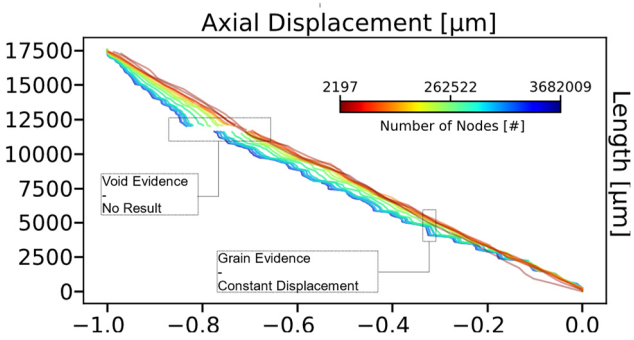

Figure 14. Axial displacement over central cutline.

5. Conclusions

This work is a brief review on the practice of mesoscale simulation concepts applied on cemented natural sand. The imaging tool of X-ray Computed Tomography is utilized to scan the initial internal geometry of the sample and quantify it in the form of a three-dimensional digital image. The information in this data structure is inspected and it was concluded that the image suffers from mild beam hardening artefacts. The correction of these artefacts is conducted by a developed image filter. Against the non-aligned grey values, the filter performs axial and radial domain decomposition and calculates correction factors, based on histogram derived equivalents. These correction factors are applied on their corresponding domains by simple addition, enlightening and equalizing the raw X-ray scan output. The post-processed image is then subjected to a cut-off filter, which assigns a specific magnitude to all the voxels of excessive brightness. This process allows the grouping of the voxels to the corresponding physical phase through the imposition of two thresholding values. The conversion of the labelled three- dimensional image to an equivalent meshed domain was carried out by applying an adaptive image meshing algorithm. This process derives the edges of all the involved inclusions and produces an equivalent adapted tetrahedral mesh, which has been validated to correspond to the image with minimal error after a certain point of nodal density. The equivalent discretized domain is then equipped with material properties derived by the bibliography on Quartz sand properties, calibrated to match the experimental uniaxial compression test and boundary conditions that reproduce the uniaxial compression. The objectivity of

the simulation was tested in terms of computational validity; a parametric study over representative results suggested that the domain becomes mesh independent after considerable discretization. Finally, the ability of the simulation to be able to produce the mesoscale granular concepts. Apparently, the quasi granular response of the material is displayed on the axial kinematic field, which considerably diverges from the uniform contour obtained by generic linear elasticity. The mesoscale enriched simulation is able to reproduce the rigid motion of grains inside the deformable cement mortar naturally, by incorporating the spatial information on the existing inclusions. A plotline inspection over this field, as captured by different mesh fineness, quantitatively shows that the capturing of granular phenomena is a quite expensive concept, demanding fine discretization, as already suggested by the computational validation conducted. Furthermore, this evidence shows that convergence is also reached for the capturing of the granular phenomena, as rigid body motion is revealed at certain accuracy.

The upgrade of the incorporated elements is the next action towards improved accuracy, which shall be performed by developing an expansion over the triangulation algorithm. Such expansion will enrich the tetrahedral elements with additional nodes on the edges, rendering them from 4 noded constant strain to 10 noded linear strain tetrahedra reforming their shape functions from linear to quadratic. This reform would allow non-linear deformation of the tetrahedron, which is required due to the shearing conditions that the mortar is subjected in the neighborhood close to the intergranular contact.

Acknowledgements

The authors acknowledge the funding of this research attempt by the German Research Foundation (Deutsche Forschungsgemeinschaft, DFG) and are grateful to Laboratoire 3SR, Grenoble for providing beam time and experimental support.

References

Airey, D. W. 1993. "Triaxial Testing of Naturally Cemented Carbonate Soil." *J. Geotech. Eng.* 119: 1379-1398. doi: https://doi.org/10.1061/(ASCE)0733-9410(1993)119:9(1379)

Alavarado, G., M. R. Coop, and S. Willson. 2012. "On the role of bond breakage due to unloading in the behaviour of weak sandstones." *Géotechnique* 62: 303-316. doi: https://doi.org/10.1680/geot.8.P.017

Alliez P., Jamin C., Rineau L., Tayeb S., Tournois J,. Yvinec M. 2022. *3D.* CGAL Editorial Board. https://doc.cgal.org/5.5/Manual/packages.html

Boissonnat J.D., Oudot S.Y. 2005. "Provably good sampling and meshing of surfaces." *Graphical Models.* doi: https://doi.org/10.1016/j.gmod.2005.01.004

Clough, W., N. Sitar, and R. C. Bachus. 1981. "Cemented Sands under Static Loading." *J. Geotech. Eng. Div.* 107: 799-817. doi: https://doi.org/10.1061/AJGEB6.0001152

Cundall, P. A., and O. D.L. Strack. 1979. "A discrete numerical model for granular assemblies." *Géotechnique* 29: 47-65. doi: https://doi.org/10.1680/geot.1979.29.1.47

Dano, D., P.Y. Hicher, and S. Tailiez. 2004. "Engineering properties of grouted sands." *J. Geotech. Geoenviron. Eng.* 130: 328-338. doi: https://doi.org/10.1061/(ASCE)1090-0241(2004)130:3(328)

Das, A., A. Tengattini, G. Viggiani, and G. Nguyen. 2014. "A thermomechanical constitutive model for cemented granular materials with quantifiable internal variables. Part II - Validation and localization analysis." *J Mech Phys Solids.* doi: https://doi.org/10.1016/j.jmps.2014.05.022

Desrues, Jacques, G. Viggiani, and P. Bésuelle. 2010. *Advances in X-ray Tomography for Geomaterials.* doi: https://doi.org/10.1002/9780470612187

Hsieh, J. 2015. *Computed Tomography: Principles, Design, Artifacts, and Recent Advances, Third Edition.* SPIE. doi: https://doi.org/10.1117/3.2197756

Moës, N., M. Cloirec, P. Cartraud, and J.-F. Remacle. 2003. "A computational approach to handle complex microstructure geometries." *COMPUT METHOD APPL M* 192: 3163-3177. doi: https://doi.org/10.1016/S0045-7825(03)00346-3

Nagula, S., J Grabe, and P. Mayanja. 2018. "Deep vibration compaction of sand using mini vibrator." *PHYSICAL MODELLING IN GEOTECHNICS.* London.

Otsu, N. 1979. "A Threshold Selection Method from Gray-Level Histograms." *IEEE Transactions on Systems, Man, and Cybernetics* 9: 62-66. doi: https://doi.org/10.1109/TSMC.1979.4310076

Pons J.P., S´egonne F., Boissonnat J.D., Rineau L., Yvinec M.,. 2007. "High-Quality Consistent Meshing of Multi-label." *Lecture Notes in Computer Science* (Springer, Berlin, Heidelberg). doi: https://doi.org/10.1007/978-3-540-73273-0-17

Rosquoët, F., A. Alexis, A. Kheilidj, and A. Phelipot. 2003. "Experimental study of cement grout: Rheological behavior and sedimentation." *Cem Concr Res* 33: 713-722. doi: https://doi.org/10.1016/S0008-8846(02)01036-0

Roubin, E., A. Vallade, N. Benkemoun, and C. Jean-Baptiste. 2014. "Multi-scale failure of heterogeneous materials: A double kinematics enhancement for Embedded Finite Element Method." *Int J Solids Struct* 52. doi: https://doi.org/10.1016/j.ijsolstr.2014.10.001

Stamati, O., E. Roubin, E. Andò, and Y. Malecot. 2018. "Phase segmentation of concrete x-ray tomographic images at meso-scale: Validation with neutron tomography." *Cem Concr Compos* 88. doi: https://doi.org/10.1016/j.cemconcomp.2017.12.011

Stamati, Olga and Andò, Edward and Roubin, Emmanuel and Cailletaud, Rémi and Wiebicke, Max and Pinzón, Gustavo and Couture, Cyrille and Hurley, Ryan and Caulk, Robert and Caillerie, Denis and Matsushima, Takashi and Bésuelle, Pierre and Bertoni, Félix and, O. Stamati, E. Andò, E. Roubin, R. Cailletaud, M. Wiebicke, G. Pinzón, et al. 2020. "spam: Software for Practical Analysis of Materials." *J. Open Source Softw.* 5: 2286. doi: https://doi.org/10.21105/joss.02286

Stamati, Olga and Roubin, Emmanuel and Andò, Edward and Malecot, Yann and Pascal, Charrier. 2021. "Fracturing process of micro-concrete under uniaxial and triaxial compression: Insights from in-situ X-ray mechanical tests." *Cement and Concrete Research* 149: 106578. doi: https://doi.org/10.1016/j.cemconres.2021.106578

Tengattini, A., A. Das, G. D. Nguyen, G. Viggiani, S. A. Hall, and I. Einav. 2014. "A thermomechanical constitutive model for cemented granular materials with quantifiable internal variables. Part I-Theory." *J Mech Phys Solids* 70: 281-296. doi: http://doi.org/10.1016/j.jmps.2014.05.021

Wichtmann, T., and T. Triantafyllidis. 2014. "Stiffness and Damping of Clean Quartz Sand with Various Grain-Size Distribution Curves." *J. Geotech. Geoenviron. Eng.* 140. doi: https://doi.org/10.1061/(ASCE)GT.1943-5606.0000977